Observation of a surface alloying-to-dealloying transition during growth of Bi on Ag(111)

K. H. L. Zhang,[1,2,*] I. M. McLeod,[3] Y. H. Lu,[1] V. R. Dhanak,[3] A. Matilainen,[4] M. Lahti,[4] K. Pussi,[4] R. G. Egdell,[2] X.-S. Wang,[1] A. T. S. Wee,[1] and W. Chen[1,5,†]

[1]*Department of Physics, National University of Singapore, 2 Science Drive 3, 117542, Singapore*

[2]*Department of Chemistry, Chemistry Research Laboratory, Mansfield Road, Oxford OX1 3TA, United Kingdom*

[3]*Department of Physics, University of Liverpool, Liverpool L69 3BX, United Kingdom*

[4]*Department of Mathematics and Physics, Lappeenranta University of Technology, P.O. Box 20, FIN-53851 Lappeenranta, Finland*

[5]*Department of Chemistry, National University of Singapore, 3 Science Drive 3, 117543, Singapore*

(Received 30 November 2010; revised manuscript received 11 April 2011; published 14 June 2011)

The atomic structures that develop as a function of coverage during deposition of Bi on Ag(111) have been studied using low-temperature scanning tunneling microscopy, low-energy electron diffraction, and *ab initio* calculations. The growth process involves two sequential stages. At low coverage, Bi atoms are incorporated into the topmost layer of Ag(111), resulting in the formation of an Ag_2Bi alloy confined to the surface and ordered $(\sqrt{3} \times \sqrt{3})R30^\circ$ Ag_2Bi islands supported on Ag(111). This mode of accommodation of Bi was found to be energetically favorable based on *ab initio* total-energy calculations. At coverage above a critical value of 0.55 monolayers, the Ag_2Bi alloy phase gradually converts into an ordered Bi $(p \times \sqrt{3})$ overlayer structure supported on Ag(111). We postulate that the dealloying transition is likely driven by compressive strain induced by incorporation of large-size Bi atoms into Ag at a high coverage and the subsequent lack of miscibility of Ag and Bi bulk phases. After completion of the dealloying process, Bi(110) thin films can be grown epitaxially on top of Ag(111) with a chemically abrupt interface.

DOI: 10.1103/PhysRevB.83.235418 PACS number(s): 68.55.−a, 68.43.−h, 68.47.−b, 68.37.−d

I. INTRODUCTION

The study of the heteroepitaxial growth of metals on metallic substrates has been motivated by the demand for high-quality thin metallic heterostructures with sharp interfaces in technological applications such as magnetic data storage and spintronics.[1–3] It is becoming clear that a wealth of complex phenomena may arise at an atomic scale that are not predicted from simple thermodynamic considerations of the respective surface and interface energies of the metal adatoms and the substrates.[4–7] Tersoff has predicted that surface-confined alloy phases may arise as an alternative to overlayer structures as a means to relieve the surface stress in systems dominated by an atomic size mismatch, even in cases where the metals are immiscible in the bulk.[8] This is particularly the case for the growth of comparatively heavier elements such as lead (Pb), antimony (Sb), and bismuth (Bi) on noble-metal surfaces.[8–13] Surface alloying is a powerful way of developing unique physical and chemical properties in alloys that do not have a bulk counterpart.[14–16] Elegant examples include the exceptionally large spin-orbit splittings of surface states in surface alloys between heavy elements such as Bi or Pb on light metals such as Cu and Ag, which opens potential applications in the area of spintronics.[17,18]

Bi is a typical group-V element and adopts a rhombohedra $A7$ lattice belonging to the space group $R\bar{3}m$. There are two atoms per unit cell, which can also be described by a hexagonal basis.[19] The band structure of Bi is that of a semimetal with an overlap of $\sim$40 meV between valence and conduction bands that arises due to a slight distortion along the trigonal axis, which is (111) in the rhombohedra basis or (0001) in the hexagonal basis. Bi possesses an unusual array of physical properties, including low carrier density, a long Fermi wavelength ($\sim$40 nm at room temperature), and high carrier mobility. Most interestingly, the low-index surfaces of Bi such as Bi(111), Bi(100), and Bi(110) show very different electronic properties from the bulk associated with spin-orbit (SO) splitting at the surface due to the breakdown of inversion symmetry (the so-called Rashba-Bychkov effect).[19–21]

It has been recently reported that submonolayer Bi on Ag(111) forms a $(\sqrt{3} \times \sqrt{3})R30^\circ$ surface alloy.[17] The $(\sqrt{3} \times \sqrt{3})R30^\circ$ structure is of particular interest because the intermixing of the size mismatched atoms and the corresponding in-plane potential variations lead to giant SO splitting, which has implications for spintronics applications.[17,22,23] Nonetheless, a detailed investigation of the atomic structures of these two-dimensional (2D) surface alloys is still lacking, even though such structural information plays a critical role in determining the in-plane potential gradient, and thus the SO splitting of the surface alloys.[24] Furthermore, a similar class of electronic states evolves by the quantum confinement of electrons in ultrathin films with a thickness comparable to the electron coherence length, to give so-called quantum well states. It has been recently reported that a giant SO splitting of quantum well states has been observed within a Bi monolayer on Cu(111).[25] Based on first-principles calculations, the authors argued that the huge SO splitting originated from the perpendicular potential at the surface and interface of the ultrathin Bi film. This finding opens the possibility of controlling the SO splitting by tuning the nanostructure of the ultrathin film.

In the present work, we present a detailed study of the nucleation of Bi on Ag(111), the subsequent development of the Ag_2Bi surface alloy, and the growth of a Bi thin film on Ag(111) using scanning tunneling microscopy (STM) and *ab initio* total-energy calculations. We show that in the initial stages of deposition Bi atoms are incorporated into the topmost Ag(111) layer by exchanging with the surface Ag atoms to form a substitutional surface alloy. This mode of incorporation was found to be energetically favorable based on *ab initio*

total-energy calculations. However, a surface dealloying process ensues with increasing Bi coverage, presumably driven by the high compressive strain induced by incorporation of larger-size Bi atoms into the Ag matrix at high concentrations. For coverages above 1 monolayer (ML), the Ag_2Bi surface alloy demixes and a highly ordered Bi(110) monolayer is formed on top of Ag(111).

II. EXPERIMENTAL AND COMPUTATIONAL METHODS

The experiments were carried out in a homebuilt multichamber ultrahigh vacuum (UHV) system with a base pressure of better than 2×10^{-10} mbar incorporating an Omicron low-temperature scanning tunneling microscope (LT-STM) stage.[26] The STM was operated with a Nanonis controller (Nanonis, Switzerland). Ag(111) substrates were cleaned by repeated cycles of Ar^+ sputtering and annealing at 800 K. The cleanliness and surface order of the samples was checked by LT-STM images, which in the final stages of cleaning showed sharp step edges and smooth terraces without obvious signs of impurities. Bi was thermally evaporated from a Knudsen cell in a growth chamber with a base pressure of better than 3×10^{-10} mbar. The Bi deposition rate was calibrated using a quartz microbalance (QCM) and was set at 0.05 ML/min, where 1 ML is defined as 1 atomic layer of Bi(110), i.e., 9.3×10^{14} atoms cm^{-2}. STM images were obtained at 77 K in constant-current mode with a chemically etched tungsten tip. Additional low-energy electron diffraction (LEED) experiments were performed in a standard UHV surface science chamber with rear view LEED optics from OCI Vacuum Microengineering.

The static calculations of total energies were performed using density functional theory (DFT) as implemented in the Vienna *ab initio* simulation package (VASP),[27,28] including the projector augmented-wave (PAW) potentials.[29] A kinetic energy cutoff of 400 eV was applied to the plane waves, which was found to produce well-converged results for both Ag and Bi. The exchange correlation potential employed the generalized gradient approximation (GGA) of the Perdew-Wang 91 (PW91).[30] A $10 \times 8 \times 1$ Monkhorst-Pack mesh was used for k-point sampling.[31] The Ag surface was modeled using a supercell approach with thin slabs separated by vacuum spacings. Periodic boundary conditions were applied to the central supercell so that it was reproduced periodically throughout xy space. The periodic slab was modeled with six layers of Ag atoms. A region of ~ 10 Å of vacuum was inserted in the z direction to prevent interactions between periodic images. The SO coupling has not been switched on in the VASP calculation. We have tested that the SO coupling did not have significant effect on the resulting structures. The bottommost layer of the surface slab was frozen during the geometry relaxation. An Ag lattice constant of 4.17 Å was used, which was obtained from bulk cell optimization using the same computational parameters.

III. RESULTS AND DISCUSSION

A. Surface alloying at low coverage

Figure 1(a) shows a large-area STM image following deposition of 0.2 ML of Bi on a clean Ag(111) surface at room temperature. It reveals dispersed protrusions (marked P), large meandering two-dimensional (2D) islands (marked LI), and small compact islands (marked SI). The high-resolution STM image of Fig. 1(b) indicates that the protrusions have a spherical shape with a diameter of ~ 4 Å. The apparent height between the protrusion and the surrounding Ag terrace is ~ 0.3 Å, as seen by the line profile in Fig. 1(c). These features are associated with Bi atoms incorporated into the topmost layer of Ag(111) by an exchange process which involves substitution of substrate Ag atoms by Bi atoms. The surface Bi protrusion is expected on the basis of a simple hard-sphere picture because the bulk metallic radii of Bi (1.56 Å) is larger than that of Ag (1.44 Å). This process results in the formation of a Bi-Ag alloy confined in the surface. It is noted that the substitutional Bi atoms are randomly distributed among the available Ag lattice sites.

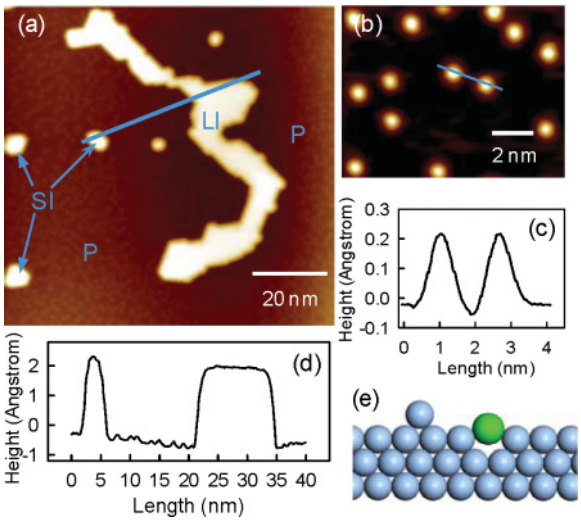

FIG. 1. (Color online) (a) An overview of large-scale STM images of 0.2 ML Bi deposited on Ag(111) ($V_s = -1.8$ V, $I_t = 0.2$ nA), showing dispersed protrusions (marked P), large meandering islands (marked LI), and small compact islands (marked SI). (b) High-resolution STM image of the disperse protrusions. (c) A line profile along the line in (b). (d) A line profile along the line in (a). (e) Schematic model for the incorporation of Bi (green) in an Ag lattice (navy).

In contrast, the line profiles in Fig. 1(d) indicate that the apparent topographic height of the meandering islands (LI) and small islands (SI) is 2.5 Å, corresponding to the height of an island one atomic layer thick. Atomically resolved STM images such as those shown in Fig. 2(a) reveal that both islands have an ordered hexagonal lattice with a $(\sqrt{3} \times \sqrt{3})R30^\circ$ superstructure ($\mathbf{a} \sim 5$ Å), where the periodicity is defined in terms of the Ag(111) substrate surface. Based on these observations, we speculate that these islands contain a 2D Bi-Ag alloy layer and that the alloy layer is formed from Ag atoms that are displaced from the surface layer by Bi atoms along with nonembedded Bi adatoms found on the Ag(111) surface. A schematic model of the proposed structure is shown in Fig. 3(a). The formation of this structure involves the following steps. First, deposited Bi atoms embed themselves into the topmost Ag layer to form a dilute substitutional alloy. One Ag atom is displaced out of the surface for each Bi atom

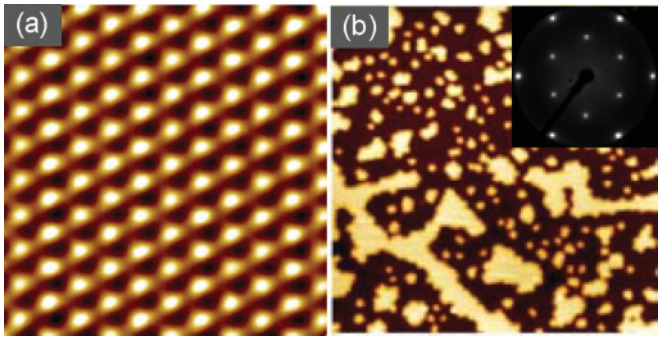

FIG. 2. (Color online) (a) High-resolution 5 nm × 5 nm STM image ($V_s = 1.2$ and $I_t = 0.18$ nA) from the top of a large meandering island, showing the supported Ag_2Bi surface alloy with an ordered $(\sqrt{3} \times \sqrt{3})R30^\circ$ superstructure (the bright spots are associated with Bi atoms). (b) Large-scale STM image (100 nm×100 nm) of 0.4 ML Bi deposited on Ag(111). The inset shows the LEED pattern of the $(\sqrt{3} \times \sqrt{3})R30^\circ$ structure with an electron beam energy of 42 eV.

that is incorporated. The Ag adatoms then diffuse and coalesce with nonembedded Bi adatoms to form the ordered Ag_2Bi alloy islands on top of Ag(111). We did not observe any pure Ag islands formed by nucleation of the displaced Ag adatoms, which indicates that these adatoms are stabilized in the form of ordered $(\sqrt{3} \times \sqrt{3})R30^\circ$ islands. Hence one might expect a direct correlation between the numbers of embedded Bi atoms and the surface area covered by $(\sqrt{3} \times \sqrt{3})R30^\circ$ islands, given that each $(\sqrt{3} \times \sqrt{3})R30^\circ$ unit cell contains one Bi and two ejected Ag atoms. Indeed, statistical analysis reveals that the

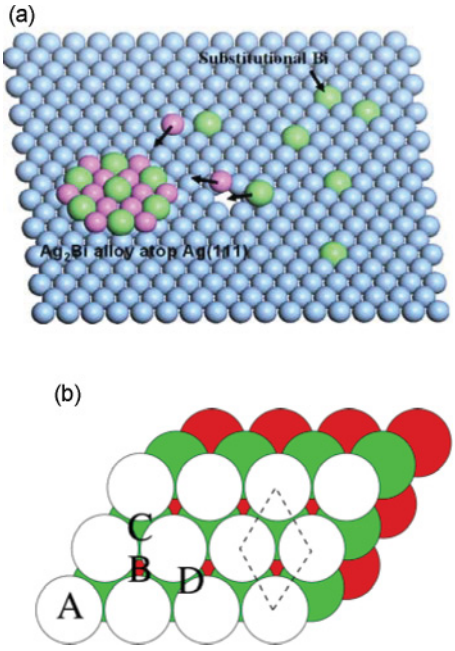

FIG. 3. (Color online) (a) Schematic of the formation of the Ag_2Bi surface alloy: Ag lattice (navy), Bi atoms (green), and squeezed Ag atoms (pink). (b) The four adsorption sites (A = top, B and C = hollow, and D = bridge) considered in DFT calculations. The corresponding adsorption energies are given in Table I. The white spheres represent the first Ag layer, the green spheres represent the layer, and the red spheres represent the third layer.

density of substitutional Bi atoms is roughly identical to the density of Ag atoms in the ordered alloy islands. Furthermore, both the density of the embedded Bi atoms and the surface area of $(\sqrt{3} \times \sqrt{3})R30^\circ$ islands increase linearly with the amount of Bi deposited. As shown in Fig. 2(b), with 0.4-ML Bi deposition most of the Ag surface is covered with Ag_2Bi surface alloy islands. At this stage a well-defined $(\sqrt{3} \times \sqrt{3})R30^\circ$ LEED pattern can be observed, as shown in the inset of Fig. 2(b).

The phenomenon of alloy formation confined to a surface layer has been identified in many other heteroepitaxial systems, including those where there is bulk miscibility such as Ag/Cu(100),[32] In/Cu(100),[33] and Au/Fe(100),[34] as well as in systems where the two components are immiscible in the bulk such as Au/Ni(110) (Ref. 4) and Sb/Ag(111).[11] According to the theoretical study by Tersoff,[8] for systems dominated by atomic size mismatch, surface strain effects can favor alloying on a surface even though strain suppresses intermixing in the bulk. Clean metallic surfaces are normally under tensile stress due to broken bonds at the surface.[34] Thus the incorporation of large atoms into the surface is an efficient way to relieve the surface tensile stress. Theoretical calculations based on the embedded atom method (EAM) indicated that Ag(111) has a tensile surface stress of 0.6 eV $Å^{-2}$.[35] Therefore, the tensile surface stress can be effectively relaxed by the incorporation of the large Bi atom (metallic radii = 1.56 Å) into the Ag (1.44 Å) lattice. This is despite the fact that the surface energy for Bi(110), $\gamma_{Bi}(110) = 0.541$ J m^{-2}, is much smaller than the surface energy for Ag(111), $\gamma_{Ag}(111) = 1.17$ J m^{-2}, which would appear to favor formation of a Bi overlayer structure on Ag(111).[36] Similar considerations also explain the preference for substitutional Bi atoms to be distributed within the Ag lattice without any clustering. Because of the larger size of Bi, the incorporation of Bi atoms into the Ag lattice can induce local strain fields, which causes two nearest-neighbor embedded atoms to repel each other in the surface. Thus the embedded Bi atoms never have Bi nearest neighbors. Recent *ab initio* studies of the 3*d* transition metals on Au(100) also showed a repulsive interaction between nearest-neighbor embedded atoms, thus explaining the random distribution of the embedded impurities.[37] By contrast, the local strain can be effectively relieved in the Ag_2Bi alloy overlayer because of the finite size of the alloy islands supported on the Ag substrate.

However, the model proposed by Tersoff takes into account only the strain energy of the system.[8] The equilibrium structure will be determined by minimization of the total energy and not just the surface strain energy. Therefore, we performed first-principles DFT calculations to compare the energies of adsorption and incorporation for Bi on Ag(111) at various sites, including on-top, hollow, and bridge adsorption sites as well substitutional sites, as indicated in Fig. 3(b).[38] The adsorption energies of Bi atom are defined as

$$E_{ads} = \frac{1}{N_{Bi}}(E_{tot} - E_{clean} - N_{Bi}E_{Bi}), \quad (1)$$

where E_{tot} is the total energy of a relaxed Ag/Bi supercell; E_{clean} is the total energy of the relaxed clean Ag slab; N_{Bi} is the number of Bi atoms and E_{Bi} is the energy of one atom in

TABLE I. Adsorption energies for different adsorption sites as indicated in Fig. 3(b).

Adsorption site	Adsorption energy (eV)
Top (A)	0.414
Hollow (B)	0.198
Hollow (C)	0.234
Bridge (D)	0.208
Surface alloy	−0.353

the bulk of the Bi metal. For substitutional alloy structures the adsorption energy is defined as

$$E_{\text{ads}} = \frac{1}{N_{\text{Bi}}}(E_{\text{tot}} - E_{\text{clean}} - N_{\text{Bi}}E_{\text{Bi}} + N_{\text{Bi}}E_{\text{Ag-bulk}}), \qquad (2)$$

where $E_{\text{Ag-bulk}}$ is the total energy of an Ag bulk atom. The adsorption energies for each site of the models that showed convergence in the calculations are listed in Table I. The fcc hollow site B is the most favorable for absorption, albeit with a small energy difference between the two possible hollow sites and the bridge sites. However, the substitutional surface alloy structure was found to be the most stable configuration, with an absorption energy of −0.353 eV. There is thus a clear preference for the occupation of substitutional sites in the surface layer. The DFT calculations also indicate that the "rumpling" of the surface alloy has an amplitude of 0.6 Å, with the Bi atoms sitting above the underlying Ag surface atoms. This is in good agreement with a recent structural determination of the $(\sqrt{3}\times\sqrt{3})R30^\circ$ surface structure of the Ag_2Bi alloy layer by the analysis of LEED curves.[38] The rumpling amplitude is larger than the apparent protrusion height measured by STM. This can be explained by the fact that the apparent height in a STM image depends on both the topographic height and the density of electronic states near the Fermi level. This amplitude is, however, smaller by ∼0.24 Å than that predicted by a simple hard-sphere model based on bulk metallic radii of 1.44 Å for Ag and 1.56 Å for Bi. This suggests a reduction in the effective radii that is similar to that found by Quinn *et al.*[12] in their LEED study of the substitutional surface alloy structure for the Pb-Ni(111) system. It has been suggested that the reduction in the effective radii may be attributed to the influence of valence electron charge smoothing and associated surface stress effects. A similar effect is possibly the case for the Bi-Ag(111) structure in our study.

B. Dealloying and the Bi overlayer structure

The Bi surface alloy saturates at coverage of 0.5 ML, which corresponds to 0.33 ML if defined in terms of atomic layers of Ag(111) with a sheet density of 1.38×10^{15} cm^{-2}. With additional Bi deposition, the Bi-Ag system undergoes a dealloying process. Figures 4(a) and 4(b) show STM images which trace the evolution of the dealloying process as the Bi coverage increases. In Fig. 4(a) the Bi coverage is slightly above the saturation limit, and a different type of island begins to appear with a lower height above the surface than the $(\sqrt{3}\times\sqrt{3})R30^\circ$ alloy islands. These are labeled DA in the figure. As will be discussed below, these different islands have $\sqrt{3}$ periodicity along the Ag[11$\bar{2}$] direction, but are incommensurate in the

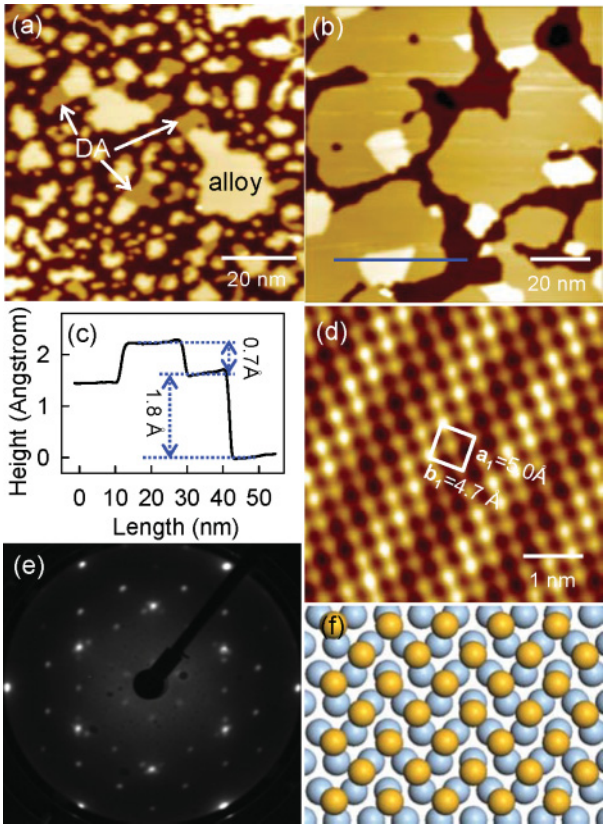

FIG. 4. (Color online) (a) Large-scale STM image of 0.6 ML Bi deposited on Ag(111), showing the appearance of $(p\times\sqrt{3})$ overlayers with a low height at the step edges of $(\sqrt{3}\times\sqrt{3})R30^\circ$ islands (labeled as "DA"). (b) The coverage of the $(p\times\sqrt{3})$ overlayers increases as 0.75 ML Bi was deposited on Ag(111). (c) A line profile along the line in (b), indicating that the height of the $(p\times\sqrt{3})$ overlayer is 1.8 Å with respect to the substituted surface alloy and 0.7 Å lower than that of the $(\sqrt{3}\times\sqrt{3})R30^\circ$ islands. (d) Atomic structure of the $(p\times\sqrt{3})$ overlayer structure with lattice constants of $\mathbf{a_1}=5.0$ Å, $\mathbf{b_1}=4.7$ Å. (e) LEED pattern (with an electron energy of 38 eV) for the $(p\times\sqrt{3})$ overlayer. (f) Schematic model for the $(p\times\sqrt{3})$ Bi overlayers (yellow) on Ag(111) (navy).

orthogonal direction. Following notation introduced by Chen *et al.*,[39] this structure is designated as $(p\times\sqrt{3})$. The authors used an electrochemical deposition technique and found that p depended on the deposition potential, hence the choice of this letter. The switchover of the structure developed further as the Bi coverage was increased to 0.75 ML [Fig. 4(b)]. Clearly, both the island size and the total coverage by the $(p\times\sqrt{3})$ overlayer islands increase dramatically, whereas the area of the $(\sqrt{3}\times\sqrt{3})R30^\circ$ islands and substitutional surface alloy decreases. Figure 4(c) shows a height profile along the line marked in Fig. 4(b), indicating that the apparent height of the $(p\times\sqrt{3})$ overlayer is 1.8 Å with respect to the substituted surface alloy and is thus 0.7 Å lower than that of the $(\sqrt{3}\times\sqrt{3})R30^\circ$ islands. A high-resolution image is shown in Fig. 4(d). This reveals the atomic structure within the $(p\times\sqrt{3})$ islands and suggests that this overlayer is based on a rectangular nonprimitive unit cell. The unit cell vectors are $\mathbf{a}_1=5.0$ Å along the Ag[11$\bar{2}$] direction and $\mathbf{b}_1=4.7$ Å along the Ag[1$\bar{1}$0] direction. Figure 4(e) shows a LEED

pattern measured with an electron energy of 38 eV for the $(p \times \sqrt{3})$ overlayer. It further confirms that the $\mathbf{a}_1$ direction of the Bi overlayer structure is commensurate with the Ag(111) surface along the Ag[11$\bar{2}$] direction ($\mathbf{a}_1 = a_{\mathrm{Ag}}\sqrt{3}$), but incommensurate along the Ag[1$\bar{1}$0] direction. Because of the threefold symmetry of the Ag(111) surface, there are three coexisting domains of the rectangular structures rotated 120° and 240° with respect to each other. The $(p \times \sqrt{3})$ overlayer structure is similar to a Bi $(p \times \sqrt{3})$ overlayer structure on Au(111) formed by electrochemical deposition.[39] The lattice constants are slightly larger than those found in the Bi(110) planes of elemental bismuth, where ($\mathbf{a}_2 = 4.74$ Å, $\mathbf{b}_2 = 4.54$ Å), so that the atomic density of 8.0×10^{14} cm^{-2} is also lower than in the Bi metal. A modulation with an amplitude of 0.2 Å is seen to be superimposed on the ordered Bi overlayer structures along the Ag[1$\bar{1}$0] direction. This modulation is straightforwardly explained as a moiré pattern arising from the interference between the Bi overlayer and the Ag substrate along the [1$\bar{1}$0] direction. We thereby identify the $(p \times \sqrt{3})$ islands as pure Bi overlayers formed during the dealloying process sitting on top of Ag(111). A structural model for the $(p \times \sqrt{3})$ overlayer based on the atomic resolution image is proposed in Fig. 4(f). At a coverage of 0.9 ML, we found that there is complete coverage of the surface by the $(p \times \sqrt{3})$ overlayer so that the dealloying process is complete.

Dealloying transitions similar to those found here have been observed in several other systems including Pd/Cu(111),[40] In/Cu(100),[32] Mn/Cu(001),[41] and Au/ Ni(110).[42] Relief of the compressive energy is proposed as one of the driving forces for the dealloying process. In the Au/Ni(110) system,[42] Au atoms initially alloy into the Ni(110) surface at low coverage but dealloy into a vacancy-stabilized Au dimer-trimer chain structure at Au coverages larger than 0.4 ML. Based on total-energy calculations it was shown that the surface compressive stress induced by the substituted Au drives the surface alloy to dealloy above a critical coverage. Similarly, in the present Ag-Bi system, the tensile stress of the clean Ag surface is originally relieved by the incorporation of large-sized Bi atoms into the Ag lattice. However, above a critical coverage, further incorporation of Bi turns the tensile stress into compressive stress. Hence, as the Bi coverage increases above the critical limit, a dealloying process is favored.

We suggest a possible mechanism for the dealloying process and formation of the $(p \times \sqrt{3})$ overlayer based on the following steps. First, starting at the step edges, the deposited Bi atoms replace the Ag atoms in the $(\sqrt{3} \times \sqrt{3})R30°$ islands on Ag(111) to form the $(p \times \sqrt{3})$ overlayer. Second, the displaced Ag atoms diffuse onto the substrate terraces and displace Bi atoms from the substitutional sites, thereby recovering the original pure Ag(111) surface. The displaced Bi atoms can add to the $(p \times \sqrt{3})$ island, playing a role similar to that of the deposited Bi atoms. We did not observe any $(p \times \sqrt{3})$ structures embedded into the terraces during STM scanning. Thus the possibility that deposited Bi atoms can replace Ag atoms in the substitutional alloy to form an embedded Bi layer can be ruled out. As a result of these processes a chemically abrupt interface can be recovered by the dealloying process.

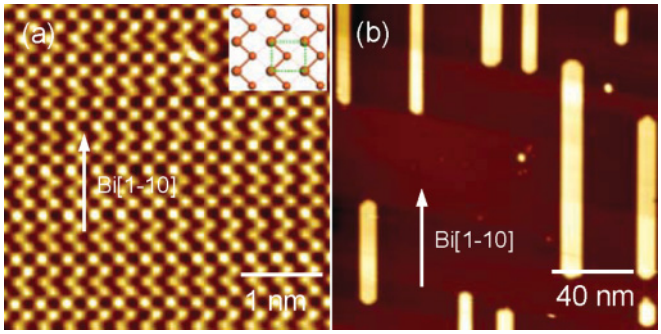

FIG. 5. (Color online) (a) Atomic resolution STM image of 1 ML Bi deposited on Ag(111), showing the formation of a Bi monolayer with the Bi(110) plane. The inset shows the atomic configuration of the Bi(110) plane. (b) STM image of 1.5 ML Bi deposition on Ag(111), showing the elongated growth along the Bi[1$\bar{1}$0] direction.

C. Bi(110) overlayers

The Bi $(p \times \sqrt{3})$ overlayer phase shows a further structural transition with increasing coverage. As shown in Fig. 5(a), after deposition of 1 ML of Bi, the lattice constants decrease compared to those discussed in Sec. III B and a rectangular unit cell with $\mathbf{a}_2 = 4.74$ Å and $\mathbf{b}_2 = 4.54$ Å can be identified in the image. The atomic density has increased to a value of 9.3×10^{14} cm^{-2}. The surface unit cell contains two atoms, and the central atom in the cell is offset to the short edge of the unit cell to give a structure containing zigzag chains. The compressed overlayer structure is basically that found on the (110) surface of elemental Bi. Based on STM and LEED observations, the epitaxial relationship between Bi(110) and Ag(111) is determined to be Bi[1$\bar{1}$0] ∥ Ag[1$\bar{1}$0] and Bi[001] ∥ Ag[11$\bar{2}$] with $7|\mathbf{a}_{\mathrm{Bi}[1\bar{1}0]}| = 11|\mathbf{a}_{\mathrm{Ag}[1\bar{1}0]}|$ and $20|\mathbf{a}_{\mathrm{Bi}[001]}| = 19|\mathbf{a}_{\mathrm{Ag}[11\bar{2}]}|$.[43] This is similar to the adsorption structure of Bi(110) thin films electrodeposited on Au(111).[44] In a simple model, the phase transition from the $(p \times \sqrt{3})$ structure to Bi(110) is determined by two competing interactions, namely, Ag-Bi substrate-overlayer interactions and Bi-Bi overlayer-overlayer interactions. In the loosely packed $(p \times \sqrt{3})$ overlayer, the Ag-Bi interaction dominates over the Bi-Bi interaction. This statement is corroborated by the fact that the $(p \times \sqrt{3})$ is locked pseudomorphically to the [11$\bar{2}$] direction of the Ag substrate. The relatively strong Ag-Bi interaction causes the Bi atoms to adopt positions determined by the Ag substrate lattice. However, with increasing Bi coverage, Bi-Bi interactions become more important and gradually become the major determinant of surface structure. Thus Bi-Bi interaction drives Bi to adopt its own lattice structure, giving rise to an incommensurate Bi(110) monolayer.

Increasing the Bi coverage to beyond 1 ML promotes the growth of Bi ribbon bilayers elongated along the [1$\bar{1}$0] direction, as shown in Fig. 5(b).[43] The preferential growth of Bi ribbons elongated along this direction results from the preferential attachment of Bi atoms to the ends of the ribbons. Bulk Bi has highly anisotropic bonding[19] and the surface structure of Bi(110) is characterized by zigzag covalently bonded atomic chains running along the [1$\bar{1}$0] direction, with weaker bonds in the orthogonal direction [the inset in Fig. 5(a)]. Therefore, Bi adatoms on the surface preferentially

attach to the ends of the ribbons, resulting in preferential growth along the Bi [$1\bar{1}0$] direction. Furthermore, the growth of Bi ribbons is quantized into double (110) layers units with a width of 6.6 Å, and the growth exhibits an even-number layer stability. This is consistent with recent observations of "magic" thicknesses in ultrathin Bi films on the Si(111) surface, where Bi(110) 2D islands with an even number of layers are dominant.[45] This stability is attributed to the energetically preferred pairing of two neighboring layers. On a bulk-terminated Bi(110) surface, 50% of surface atoms have *pz* dangling bonds. In a film with an even number of (110) layers, the dangling bonds are completely saturated by pairing with a neighboring layer. All the atoms are then threefold coordinated, leading to stabilization of the (110) surface. In contrast, films with an odd number of layers are not stable since the dangling bonds of the top layer are unable to be saturated by layer pairing.

IV. CONCLUDING REMARKS

In summary, we have investigated the coverage-dependent growth of Bi on Ag(111) and have identified a number of atomically ordered structures. The system exhibits an alloying and dealloying process that is typical for metal-on-metal systems where the individual components are not miscible as bulk phases. It is energetically favorable for the initially deposited Bi atoms to be incorporated into the topmost Ag(111) layer by exchanging with surface Ag atoms to form a dilute array of substitutional Bi atoms within the Ag matrix as well as an adlayer of the Ag_2Bi surface alloy. Since the incorporation of larger-sized Bi atoms presumably induces a compressive strain, a surface dealloying process ensues when the Bi coverage is reaches a critical value. Future stress measurements or kinetic Monte Carlo calculations are required to elucidate the mechanisms and driving force for the dealloying process. Nevertheless the Ag_2Bi alloy phase gradually converts into an ordered $(p \times \sqrt{3})$ overlayer structure with a rectangular lattice 2D surface cell with $\mathbf{a}_1 = 5.0$ Å, $\mathbf{b}_1 = 4.7$ Å supported on Ag(111). After the dealloying process is complete, Bi(110) thin films can be finally grown epitaxially on Ag(111) with a chemically abrupt interface. The "rumpling" of the surface alloy determined from experimental and *ab initio* calculations may provide additional information necessary to understand the giant spin splitting recently observed in the Bi/Ag(111) surface alloy system, which was believed to originate from a strong in-plane gradient of the crystal potential in the surface layer. This also provides a model system to envision the alloying process in other systems such as Pb on Ag(111), which exhibit a large Rashba effect. The ultrathin Bi films on Ag(111) may exhibit unusual properties originating from quantum confinement effects coupled with the unique properties of the Bi surface, opening up potential applications in spintronic devices.[19,25] As an elegant example, the quantum well state confinement by the ultrathin Bi film can induce a huge SO splitting. From a fundamental point of view, the results contribute further to the understanding of surface and interface phenomena in heteroepitaxial growth in materials.

ACKNOWLEDGMENT

The authors acknowledge support from Singapore ARF Grants No. R-143-000-392-133, No. R-143-000-406-112, and No. R-143-000-440-112, and from NUS YIA Grant No. R-143-000-452-101.

*hongliang.zhang@keble.ox.ac.uk
†phycw@nus.edu.sg

[1] M. Wuttig and X. Liu, *Ultrathin Metal Films*, Springer Tracts in Modern Physics Vol. 206 (Springer, New York, 2004).
[2] V. A. Shchukin and D. Bimberg, Rev. Mod. Phys. **71**, 1125 (1999).
[3] J. V. Barth, G. C. Costantini, and K. Kern, Nature (London) **437**, 671 (2005).
[4] L. Pleth Nielsen *et al.*, Phys. Rev. Lett. **71**, 754 (1993).
[5] H. Röder, E. Hahn, H. Brune, J. Bucher, and K. Kern, Nature (London) **366**, 141 (1993).
[6] H. L. Meyerheim, D. Sander, N. N. Negulyaev, V. S. Stepanyuk, R. Popescu, I. Popa, and J. Kirschner, Phys. Rev. Lett. **100**, 146101 (2008).
[7] J. A. Venables, G. D. T. Spiller, and M. Handbücken, Rep. Prog. Phys. **47**, 399 (1984).
[8] J. Tersoff, Phys. Rev. Lett. **74**, 434 (1995).
[9] J. Dalmas, H. Oughaddou, C. Leandri, J. M. Gay, G. Le Gay, G. Treglia, B. Aufray, O. Bunk, and R. L. Johnson, Phys. Rev. B **72**, 155424 (2005).
[10] H. Y. Xiao, X. T. Zu, X. He, and F. Gao, Chem. Phys. **325**, 519 (2006).
[11] S. A. de Vries, W. J. Huisman, P. Goedtkindt, M. J. Zwanenburg, S. L. Bennett, I. K. Robinson, and E. Vlieg, Surf. Sci. **414**, 159 (1998).
[12] P. D. Quinn, C. Bittencourt, and D. P. Woodruff, Phys. Rev. B **65**, 233404 (2002).
[13] G. Bihlmayer, S. Blügel, and E. V. Chulkov, Phys. Rev. B **75**, 195414 (2007).
[14] F. Besenbacher *et al.*, Science **279**, 1913 (1998).
[15] M. L. Plummer, J. van Ek, and D. Weller, *The Physics of Ultra-High-Density Magnetic Recording* (Springer, New York, 2001).
[16] V. R. Stamenkovic *et al.*, Nat. Mater. **6**, 241 (2007).
[17] C. R. Ast, J. Henk, A. Ernst, L. Moreschini, M. C. Falub, D. Pacilé, P. Bruno, K. Kern, and M. Grioni, Phys. Rev. Lett. **98**, 186807 (2007).
[18] L. Moreschini, A. Bendounan, H. Bentmann, M. Assig, K. Kern, F. Reinert, J. Henk, C. R. Ast, and M. Grioni, Phys. Rev. B **80**, 035438 (2009).
[19] Ph. Hofmann, Prog. Surf. Sci. **81**, 191 (2006).
[20] Y. Koroteev, G. Bihlmayer, J. E. Gayone, E. V. Chulkov, S. Blügel, P. M. Echenique, and Ph. Hofmann, Phys. Rev. Lett. **93**, 046403 (2004).
[21] T. Hirahara *et al.*, Phys. Rev. Lett. **97**, 146803 (2006).
[22] C. R. Ast *et al.*, Phys. Rev. B **75**, 201401(R) (2007).
[23] H. Mirhosseini *et al.*, Phys. Rev. B **79**, 245428 (2009).

[24]I. Gierz, B. Stadtmüller, J. Vuorinen, M. Lindroos, F. Meier, J. H. Dil, K. Kern, and C. R. Ast, Phys. Rev. B **81**, 245430 (2010).
[25]S. Mathias *et al.*, Phys. Rev. Lett. **104**, 066802 (2010).
[26]K. H. L. Zhang, H. Li, H. Y. Mao, H. Huang, J. Ma, Andrew T. S. Wee, and W. Chen, J. Phys. Chem. C **114**, 11234 (2010).
[27]G. Kresse and J. Hafner, J. Phys. Condens. Matter **6**, 8245 (1994).
[28]G. Kresse and J. Joubert, Phys. Rev. B **59**, 1758 (1999).
[29]P. E. Blöchl, Phys. Rev. B **50**, 17953 (1994).
[30]J. P. Perdew and Y. Wang, Phys. Rev. B **45**, 13244 (1992).
[31]H. J. Monkhorst and J. D. Pack, Phys. Rev. B **13**, 5188 (1976).
[32]P. T. Sprunger, E. Lægsgaard, and F. Besenbacher, Phys. Rev. B **54**, 8163 (1996).
[33]T. Nakagawa, S. Mitsushima, H. Okuyama, M. Nishijima, and T. Aruga, Phys. Rev. B **66**, 085402 (2002).
[34]M. M. J. Bischoff, T. Yamada, A. J. Quinn, R. G. P. van der Kraan, and H. van Kempen, Phys. Rev. Lett. **87**, 246102 (2001).
[35]R. C. Cammarata, Prog. Surf. Sci. **71**, 1 (1994).
[36]L. Vitos, A.V. Ruban, H. L. Skriver, and J. Kollár, Surf. Sci. **411**, 186 (1998).
[37]V. S. Stepanyuk and W. Hergert, Phys. Rev. B **62**, 7542 (2000).
[38]I. M. McLeod, V. R. Dhanak, A. Matilainen, M. Lahti, K. Pussi, and K. H. L. Zhang, Surf. Sci. **604**, 1395 (2010).
[39]C. Chen, K. D. Kepler, A. A. Gewirth, B. M. Ocko, and J. Wang, J. Phys. Chem. **97**, 7290 (1993).
[40]C. Nagl, O. Haller, E. Platzgummer, M. Schmid, and P. Varga, Surf. Sci. **321**, 237 (1994).
[41]W. Pan, R. Popescu, H. L. Meyerheim, D. Sander, O. Robach, S. Ferrer, M.-T. Lin, and J. Kirschner, Phys. Rev. B **71**, 174439 (2005).
[42]L. Pleth Nielsen, F. Besenbacher, I. Stensgaard, E. Lægsgaard, C. Engdahl, P. Stoltze, and J. K. Nørskov, Phys. Rev. Lett. **74**, 1159 (1995).
[43]H. L. Zhang,W. Chen, X. S. Wang, J. Yuhara, and A. T. S. Wee, Appl. Surf. Sci. **256**, 460 (2009).
[44]C. A. Jeffrey, S. H. Zheng, E. Bohannan, D. A. Harrington, and S. Morin, Surf. Sci. **600**, 95 (2006).
[45]T. Nagao, J. T. Sadowski, M. Saito, S. Yaginuma, Y. Fujikawa, T. Kogure, T. Ohno, Y. Hasegawa, S. Hasegawa, and T. Sakurai, Phys. Rev. Lett. **93**, 105501 (2004).